nature climate change

SUPPLEMENTARY INFORMATION

https://doi.org/10.1038/s41558-019-0637-z

In the format provided by the authors and unedited.

Amplified Rossby waves enhance risk of concurrent heatwaves in major breadbasket regions

Kai Kornhuber[1,2,3]*, Dim Coumou[4,5], Elisabeth Vogel[6], Corey Lesk[7], Jonathan F. Donges[5,8], Jascha Lehmann[5] and Radley M. Horton[7]

[1]Earth Institute, Columbia University, New York, NY, USA. [2]Atmospheric, Oceanic and Planetary Physics, University of Oxford, Oxford, UK. [3]National Centre for Atmospheric Science, Leeds, UK. [4]Institute for Environmental Studies, VU University Amsterdam, Amsterdam, the Netherlands. [5]Earth System Analysis, Potsdam Institute for Climate Impact Research, Member of the Leibniz Association, Potsdam, Germany. [6]Australian-German Climate & Energy College, The University of Melbourne, Melbourne, Victoria, Australia. [7]Columbia University, Lamont Doherty Earth Observatory, Palisades, NY, USA. [8]Stockholm Resilience Centre, Stockholm University, Stockholm, Sweden. *e-mail: kk3397@columbia.edu

Supplementary Materials for

Amplified Rossby waves enhance risk of concurrent heatwaves in major breadbasket regions

Kai Kornhuber[1,2,3]*, Dim Coumou[4,5], Elisabeth Vogel[6], Corey Lesk[7], Jonathan F. Donges[5,8], Jascha Lehmann[5], Radley M. Horton[7]

[1]Earth Institute, Columbia University, New York, United States
[2]Atmospheric, Oceanic and Planetary Physics, University of Oxford, Oxford, United Kingdom
[3]National Centre for Atmospheric Science, United Kingdom
[4]Institute for Environmental Studies, VU University Amsterdam, Netherlands
[5]Earth System Analysis, Potsdam Institute for Climate Impact Research, Member of the Leibniz Assoc., Germany
[6]Australian-German Climate & Energy College, The University of Melbourne, Australia
[7]Columbia University, Lamont Doherty Earth Observatory, Palisades, New York, United States
[8]Stockholm Resilience Centre, Stockholm University, Sweden

*e-mail: kk3397@columbia.edu

Data

Meridional wind fields (300 mb) and near-surface air temperature fields were obtained from the NCEP/NCAR reanalysis (*1*). These are provided on a 2.5 x 2.5 grid, limited to the satellite-based period (1979 – 2018). Results are robust against the choice of reanalysis dataset and chosen period (not shown).

5-year average commodity crop yield data (t/ha) and harvested area fraction for maize, rice, wheat and soybean for 2003-2007 is based on data from Ray et al (*2*) (retrieved from http://www.earthstat.org/) on a 5 minute by 5 minute grid.

Nutrition data for maize, rice, wheat and soybean used for generating the results shown in Fig. 5 was taken from the United States Department of Agriculture, Agricultural Research Service (USDA) database (https://fdc.nal.usda.gov ; maize: ndbNumber:20014, rice: ndbNumber:20040, wheat: ndbNumber:20076, soybean: ndbNumber:16108).

National annual yield data for Fig. 5 is based on the 'cereal, total' dataset from the Food and Agriculture Organization of the United Nations (FAO, freely available online at: http://www.fao.org/faostat/en/#home). This dataset includes the 16 most important global cereal crops, including maize, wheat, rice, and barley. For further information on this dataset see: http://www.fao.org/es/faodef/fdef01e.htm.

Methods

Wave amplitudes and phase positions: Wave amplitudes and phases are determined by applying fast Fourier transformation on the weekly averaged mid-latitudinal mean (37.5°N – 57.5°N) meridional wind velocities at the 300mb level. A Fourier transformation decomposes the meridional wind into its basic components provided by sine functions: $\Psi = \mathrm{A} \cdot \sin(kx - \varphi)$, dependent on amplitude *A*, wavenumber *k*, longitude *x* and phase φ. While wavenumber *k* refers to the number of ridges and troughs a Rossby wave would exhibit around the globe, the amplitude *A* provides a notion of how dominant a respective wavenumber is. Phase φ describes the shift with respect to a reference longitude, which in our case is given by the 180° dateline. In our analysis we focus on wavenumbers 5-8 as the associated wavelengths are of synoptic scale and thus relevant for large scale mid latitude weather patterns.

Wave events: Wave events are defined by a 1.5 σ threshold determined based on 520 weekly values June – August (13 weeks a year) for the 1979-2018 period. For wave-5-8 we detect N=45, 47, 44, 46 events respectively. For a time-series of wave-5 and wave-7 events see Fig. S8.

Temperature anomalies: Near-surface air temperature anomalies were determined by subtracting the linear trend per grid-point and day-of-year, thereby removing the climatological seasonal cycle and temperature trend before calculating weekly means.

Defining affected regions: Regions were defined by clusters of adjacent grid-points (on a 2.5°x2.5° grid) on land area that show statistically significant (p-value < 0.05) temperature anomalies during wave events (see Fig. 3a for wave-5 and Fig. 4a for wave-7). Three regions are identified for each wave number respectively. For wave-5 those are Central North America (CNA, 93 grid-points), Eastern Europe (EEU, 57 grid-points) and Eastern Asia (EAS, 24 grid-points). For wave-7, those are Western/Central North America (WCNA, 40 grid-points), Western Europe (WEU, 24 grid-points) and Western Asia (WAS, 54 grid-points). To further motivate the choice of regions, we generate one-point surface temperature coincidence maps with the central grid-point x of each of the six regions. We use a local temperature threshold $T= 1\sigma$ to generate the event time-series for each given grid-point and calculate coincidence statistics with the central grid point x (see Fig. S3 for a map of Northern hemisphere σ-values in JJA). During normal weeks with respect to waves-5 and 7, the grid-points with highest coincidence rates are localized around the central grid-point x (Fig. S4). During weeks of high amplitude wave-5 and 7 a wave-like pattern emerges across the mid-latitudes (Fig. S5). Areas with the highest coincidence rates are in good agreement with the regions selected for each wave respectively (Fig. 3a, Fig. 4a). When calculating coincidence maps for a grid-point far away from an identified region, the wave patterns are absent (not shown).

Event coincidence analysis: Event coincidence analysis (ECA) was performed using the *Coincalc R*-package by Siegmund et al (*3*) following the methodology introduced by Donges et al (*4*). Statistical significance of coincidence rates was tested using a Monte Carlo approach based on random shuffling of events in time (N=1000), employing a confidence level of 99% and 95% respectively. ECA is conceptually related to simple Bayes approaches, but allows for a refined analysis by the possibility of accounting for different time window sizes for counting coincidences, time delays or conditional coincidences.

Aggregating crop production anomalies: We employed the Superposed Epoch Analysis (SEA), also known as *compositing*, following the methodology outlined in Lesk et al (*5*). SEA has been introduced as a statistical method to isolate the signal of particular events in noisy time series data. Here we use SEA to test the influence of wave events on annual national crop production, aggregated across the countries that fall into the affected regions (see lists below), as well as a hemispheric aggregation including all countries with affected regions, globally. We estimate the composite production anomaly for wave event years by averaging standardized crop production anomalies across all years during which a wave event occurs and over all countries within a regional group. Crop production anomalies for a given country and event year were calculated as the deviation from a 7-year window mean centered around the event year, omitting the event itself from the mean, and dividing the resulting anomaly by this mean. For example, assuming 2000 is a year with a wave event, the production anomaly for this year and a given country is calculated as the production of 2000 minus the mean production of 1997-1999 and 2001-2003, divided by the mean production of the same six years. This approach provides standardized production anomalies (in %) for all countries and wave-event years. Thus, the last three years of the time-series (2015-2018) are omitted from the analysis. We estimate the composite by averaging crop production anomalies across the regional aggregations, and we present the anomalies as relative to years in which no wave events occurred, by subtracting the average production anomaly in zero-event years from the signal in years with one or more than one wave event.

Uncertainty estimates of production anomalies: The uncertainty in the composite estimate is determined by repeating the SEA procedure on the production data using randomly sampled zero-event years as well as years with one or more than one wave event, generating 100 sets of composites for zero-event years as well as event years. Each bootstrap is based on a random sub-sample (without replacement) of the observed zero-event years as well as years with one or more than one wave event, and has a sample size of 0.9 of the original number of years, i.e. 10% of years were left out in each bootstrapped sample. Based on the resampled control composites, the uncertainty around the composite production anomaly is computed across all regions as well as for each region separately. This is done for each wave respectively.

Statistical significance of production anomalies: In addition to the estimating the uncertainty bounds we performed a statistical significance analysis of the crop production anomalies during wave events using bootstrapping. For each bootstrap sample, we reshuffled the wave events across the years so the overall number of 0-, 1-, >1-event years is equal to the observations, but the years are randomly distributed. Using SEA, we calculated the composite production anomalies for 0-, 1- and >1-event years in this random sample. We subsequently calculated the difference in composite production anomalies for 1-event minus 0-event years as well as >1-event minus 0-event years, as we did for observations (globally and for regions). By repeating these steps (N=500), we obtain an empirical distribution of the differences in production anomalies between zero-event and wave-event years. We then compare the magnitude of the observed difference in production (relative to zero-event years) to this empirical distribution by determining its percentile. If the production anomaly (relative to zero-event years) is smaller than the 5th (or 10th) percentile of the production anomalies in the empirical distribution, we consider it significantly negative (i.e., we applied a one-sided statistical test to determine the significance of negative anomalies).

Assessed regions: National crop production datasets were grouped according to identified regions.

For wave-5 that is: **Central North America (CAN):** 'Canada', 'United States of America'; **Eastern Europe (EEU)**: 'Greece', 'Bulgaria', 'Moldova', 'North Macedonia', 'Ukraine', 'Romania', 'Serbia', 'Albania'; **Eastern Asia (EAS):** 'Mongolia', 'Russia', 'China'.

For wave-6 that is: **North America (NA):** 'Canada', **Central Europe:** 'Albania', 'Greece', 'Poland', 'Lithuania', 'Croatia', 'Slovakia', 'Romania', 'Serbia', 'Bulgaria', ' North Macedonia', 'Kosovo'

For wave-7 that is: **Western Central North America (WCNA)**: 'Canada', 'United States of America'; **Western Europe (WEU):** 'France', 'Switzerland', 'Spain', 'Portugal', 'United Kingdom', 'Belgium', 'Netherlands', 'Germany'; **Western Asia (WAS):** 'Turkey' ,'Iran', 'Iraq', 'Armenia', 'Azerbaijan', 'Georgia', 'Russia', 'Kazakhstan'.

For Wave-8 that is**: Western Europe (WEU)**: 'Spain', 'France', 'Belgium', **Western Asia (WAS)**: Russia, Turkey, Mongolia.

Supplementary figures

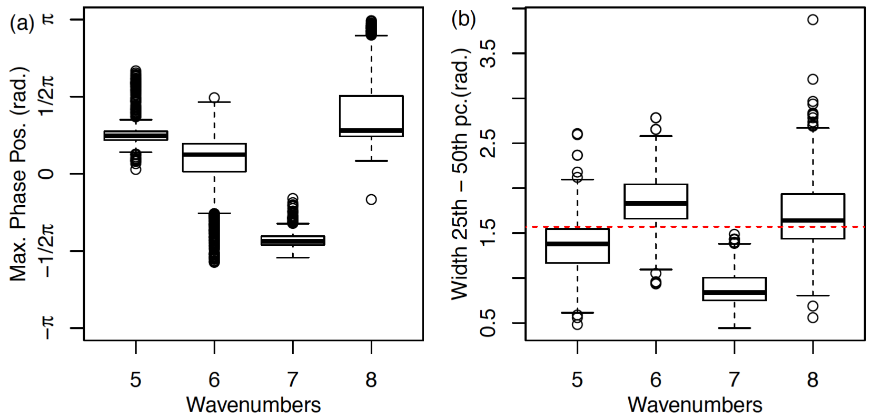

Figure S1: **Sensitivity analysis of the phase probability distribution. (a)** Distributions of the peak / maximum of the probability density distribution generated by resampling high amplitude wave events (1000 samples) shown as boxplots. Boxes refer to the 25th and 75th percentile and whiskers to the (lower) upper quartile +(-) 1.5 times the interquartile range. Outliers are shown as hollow circles. Wave-5 and wave-7 have the narrowest distributions: The position of the maximum probability is most robust. **(b)** Distributions of the distance between the 25th and 75th percentile generated from the same set of resampled wave events. Wave-5 and wave-7 have the narrowest phase position. The red dashed line refers to 1/2 π for orientation.

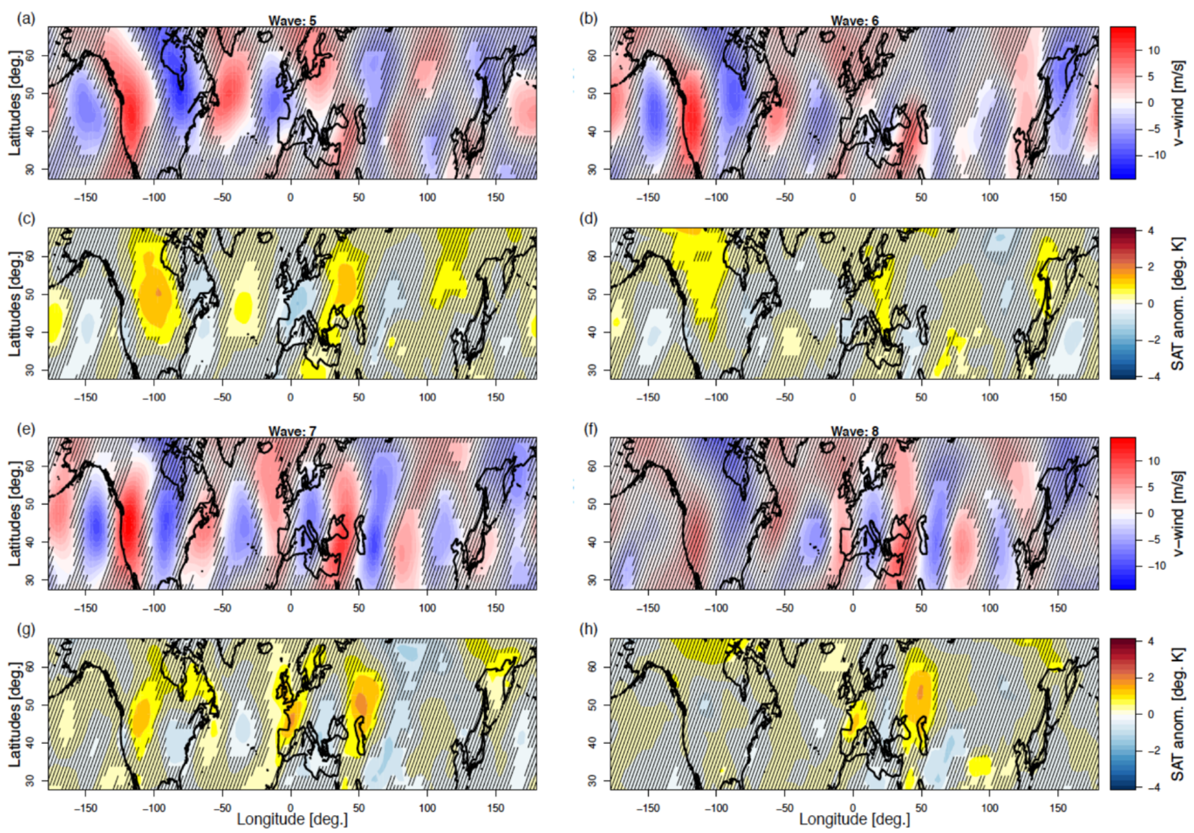

Figure S2. Teleconnections associated with waves 5 – 8. (a,b,e,f) Composites of meridional winds during weeks of high amplitude waves 5-8 (> 1.5σ) in JJA. Grid-points that are not statistically significant are masked by hatching (p>0.05). Waves 5 and 7 show a narrow one-peak phase distribution (Fig. 1) and are associated with a zonally elongated pattern of alternating meridional winds stretching around the entire hemisphere. **(c,d,g,h)** Composite temperature anomaly fields during weeks of high amplitude wave 5 – 8 (> 1.5σ) in JJA. Grid-points that are not statistically significant are masked. A circumglobal teleconnection is formed by wave-5, associated with above temperatures in Central North America, Eastern Europe and East Asia, and below average temperatures in Central Europe, and Central Asia. Wave-7 is associated with above average temperatures in Western North America, Central Europe and the Western Asia and the Japanese Sea and below average temperatures in Eastern US and SE Europe.

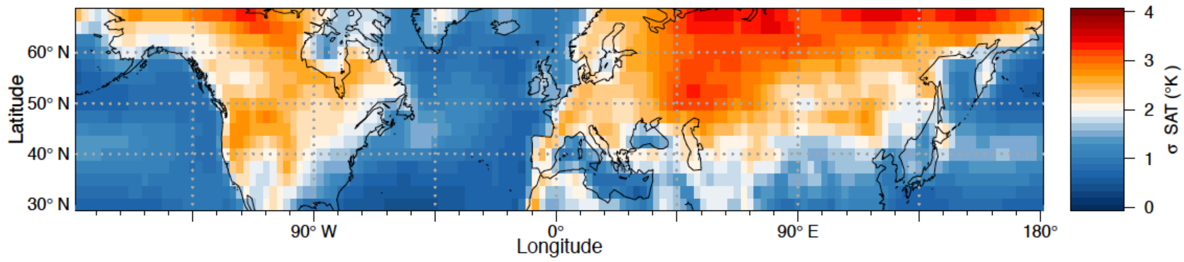

Figure S3. Standard deviation σ of northern hemisphere surface air temperature anomalies in JJA (1979 – 2018).

Robustness test of identified regions

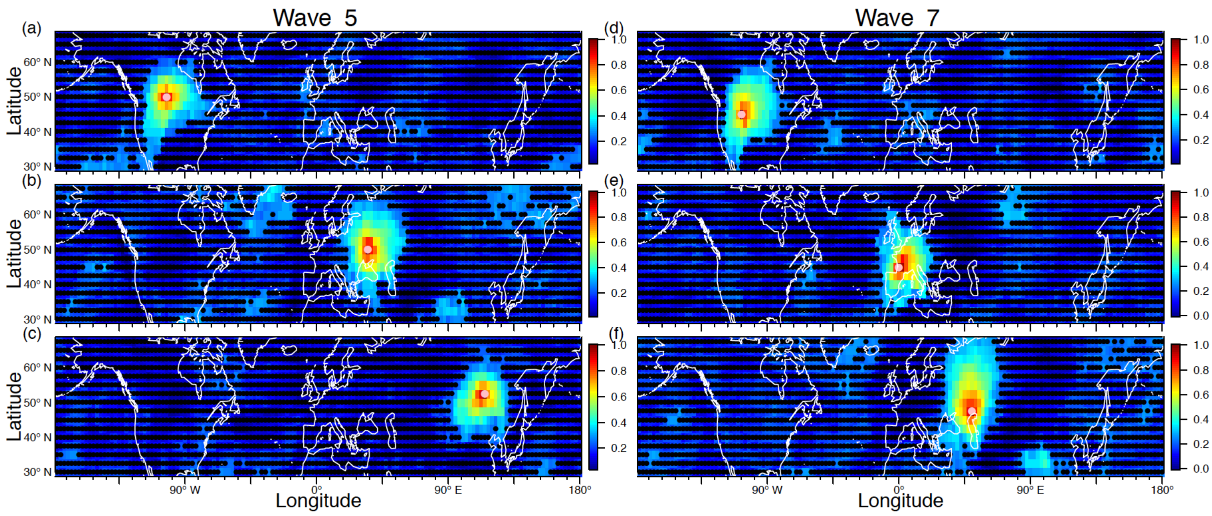

Figure S4. One-point coincidence map during weeks of low amplitudes. One-point coincidence of heat events (> 1 σ) relative to a reference point (marked in pink) placed at the center of regions associated with heat anomalies for **(a-c)** wave-5 and **(d-f)** wave-7 during weeks of normal wave amplitude (<1.5 σ). Non-significant grid-points are masked. Significance is tested based on a Poisson distribution (reps=1000, p-value < 0.01). Grid-points of highest coincidence rates are localized around the reference point.

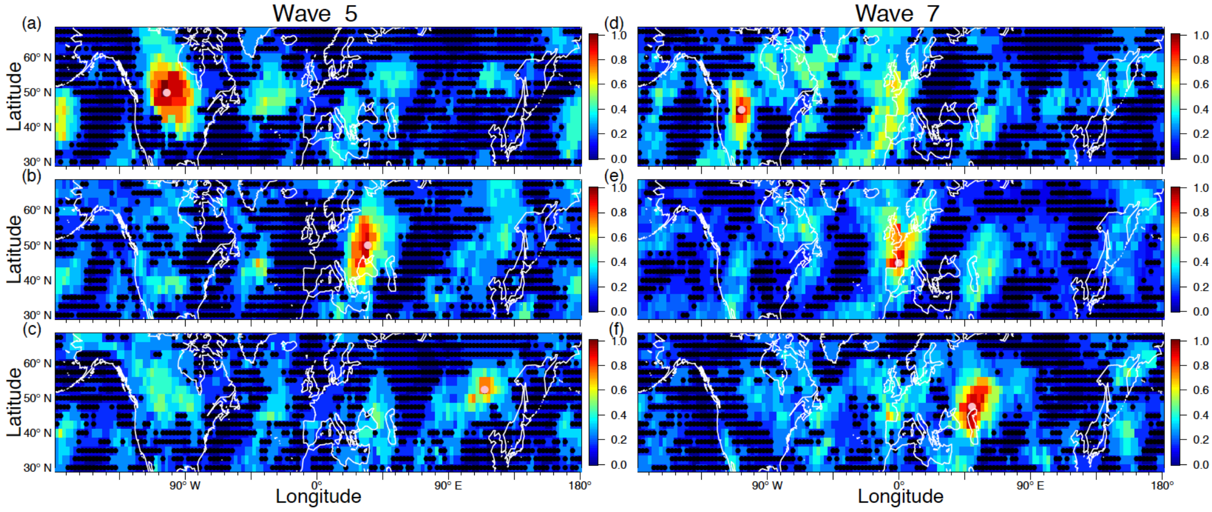

Figure S5. One-point coincidence map during weeks of high amplitudes. Same as in Fig. S4 but for weeks of high amplitude **(a-c)** wave-5 and **(d-f)** wave-7. In contrast to the maps shown in Fig. S4, coincident rates form a hemispheric pattern across the mid-latitudes. Values are highest in regions that have been identified as teleconnected regions in Fig. 2b.

To test the robustness of these results, we analyse the composite maps of simultaneous heat events in all regions ($h_{s>0.2,T>1}$) irrespective of wave amplitudes (Fig. S6). We find that v-wind and SAT anomaly fields largely resemble those shown in Fig. 2. We further find that during those events, wave amplitudes of wave-5 and 7 dominate the spectrum, while their phase position is within their preferred phase presented in Fig. 1 (Fig. S7).

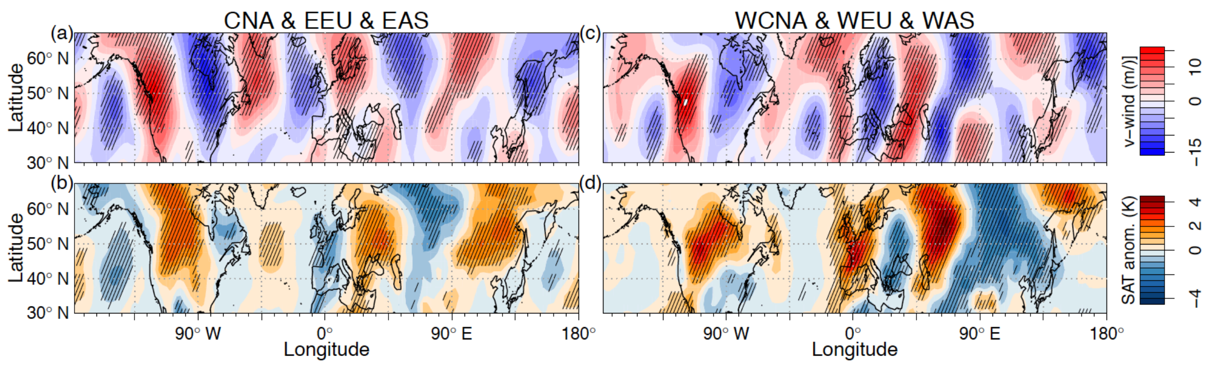

Figure S6. Composite fields during simultaneous heat events. Composite fields of **(a,d)** meridional winds, **(b,d)** temperature anomalies for simultaneous heat events ($T > 1\,\sigma$, $s > 0.2$) in regions associated with heat for **(a,b)** wave-5 (CAN, EEU, EAS; N=18) and **(c,d)** wave-7 (WCNA, WEU, WAS; N=14). Statistical significance is indicated by hatching (p≤0.05). Meridional winds exhibit a hemispheric wave-pattern of respective wavenumber similar to Fig. 2. A timeseries of the analysed events is provided in Fig. S9.

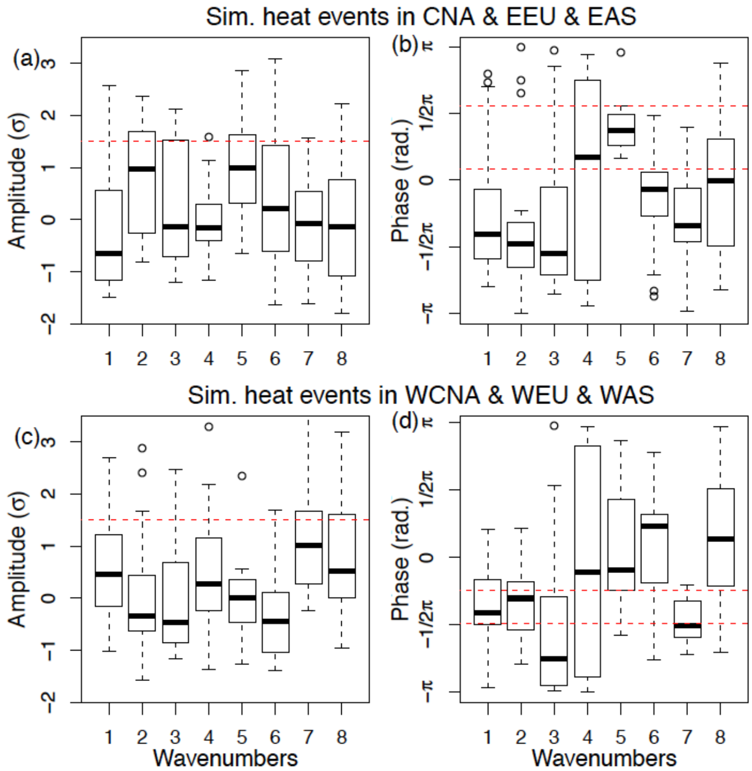

Figure S7. Wave spectra and phases during simultaneous heat events. (a) Average wave amplitudes in units of σ and **(b)** mean phase position for wavenumbers 1-8 during simultaneous heat events ($t > 1\ \sigma$, $s > 0.2$) in each region CNA, EEU and EAS. In (a) the 1.5 σ level is marked by a red dashed line while two red dashed lines mark the 25th -75th range in the waves preferred position. Wave-5 is dominating the wave spectrum, while its phase is confined to the preferred range. **(c)** Average amplitudes in units of σ and **(d)** mean phase position for wavenumbers 1-8 during simultaneous heat events WCNA, WEU and WAS. Wave-7 dominates the spectrum and is confined to its preferred phase position.

Annual time-series (June - August)

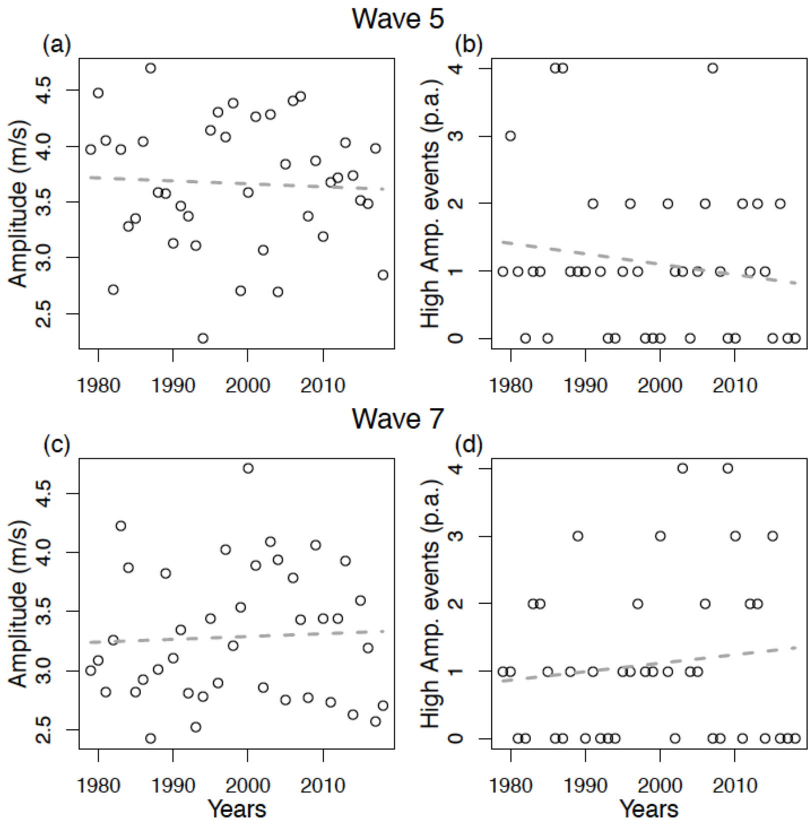

Figure S8. Timeseries of wave-5 and wave-7 annual mean amplitudes and number of high amplitude events in JJA. (a,c) Annual mean amplitude based on weekly means in JJA (1979-2018). **(b,d)** Number of high amplitude (>1.5 σ) events per year. Linear trends are provided by a grey dashed line.

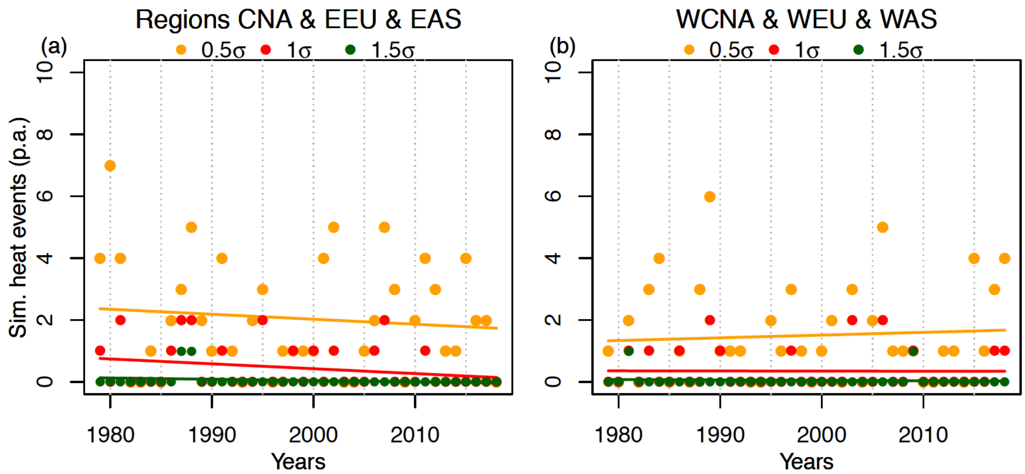

Figure S9. Timeseries of simultaneous heatwaves for teleconnected regions. Annual number simultaneous heat events in **(a)** CAN, EEU and EAS and in **(b)** WCNA, WEU and WAS (JJA, 1979-2018) for temperature anomalies T above 0.5 σ (orange), 1 σ (red) and 1.5 σ (green) with $s > 0.2$ in each region. Linear trends are provided by solid lines.

Providing numbers of total detected heat events and coinciding wave and heat events

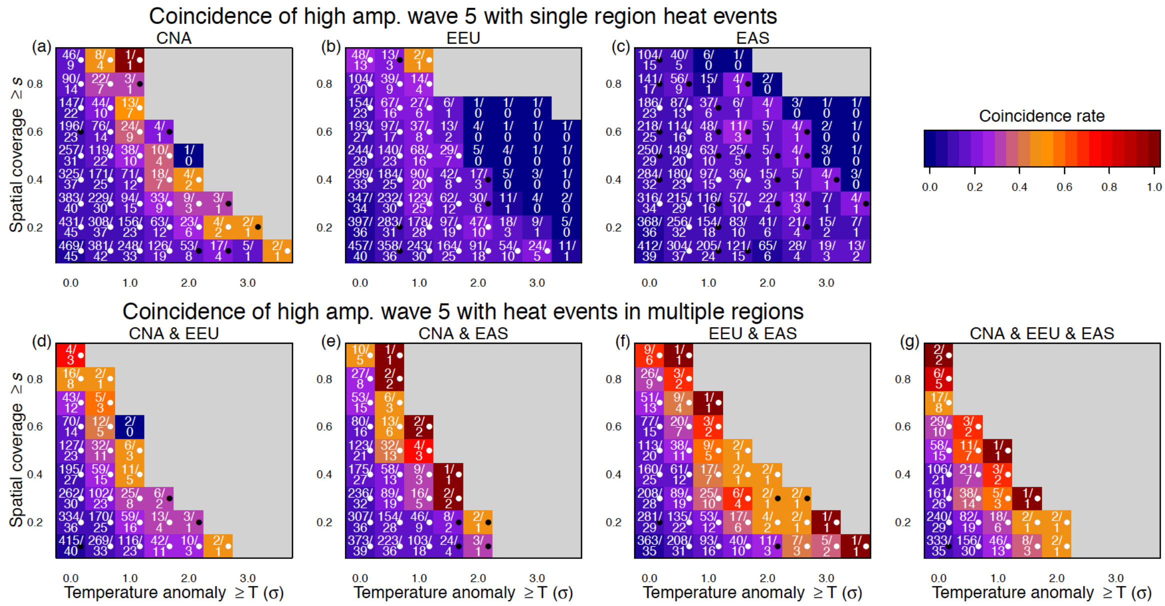

Figure S10. Coincidence of heatwaves in regions teleconnected by wave-5. (a-d) Regional coincidence rates of amplified wave-5 conditions with heat events of different intensity and spatial extent. The most severe heat events can be found in the upper right corner of each plot. The total number of heat events (upper) and total number of events coinciding with wave-5 events (lower) are provided in each tile. Statistical significance at the 99% (95%) confidence level is marked with a white (black) dot. **(d-)** As in (b-h) but for simultaneous heat events in two regions. **(g)** Coincidence rates based on all three identified regions.

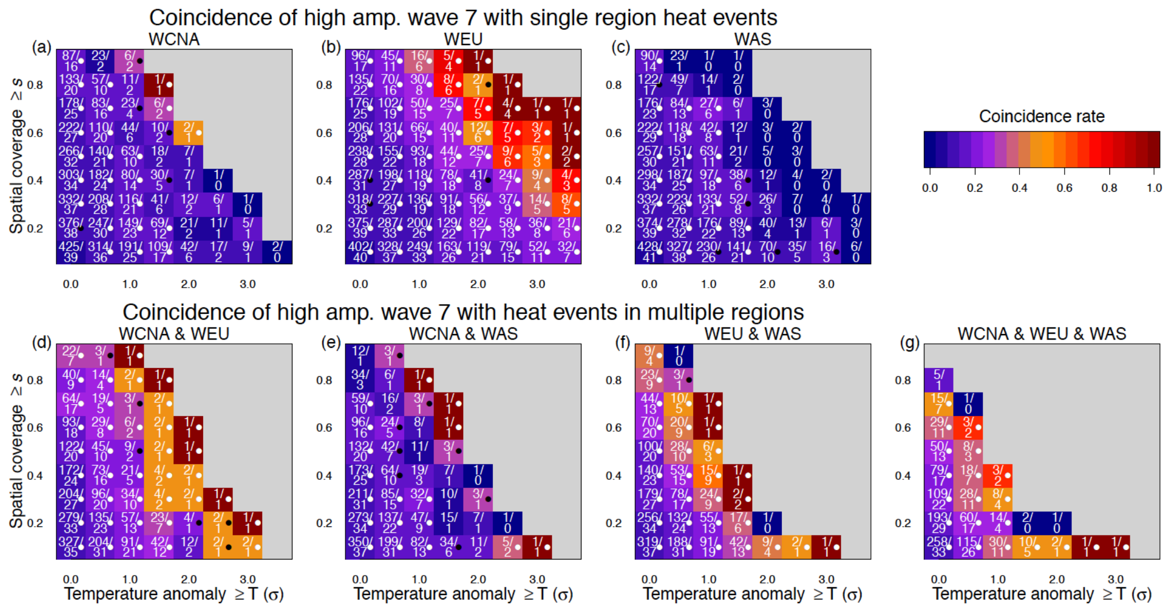

Figure S11. Coincidence of heatwaves in regions teleconnected by wave-7. As in Fig. S10, but for wave-7 and associated regions.

Coincidence of heat events in identified regions, conditioned by wave events

An alternative approach to the one presented in Figs. 3 and 4 is to compare coincidence rates of heat waves under the *condition* of high (normal) wave amplitude A_w ($\neg A_w$), e.g. $ECA(h_{s,t}|A_w, h_{s,t}|A_w)$ vs. $ECA(h_{s,t}|\neg A_w, h_{s,t}|\neg A_w)$. Thus, in contrast to the analysis presented in Figs. 3 and 4, coincidence is not assessed between (co-occurring) heat events and wave-events but between two heat events. This is done twice: first for those heat events that also fall together with a wave event, i.e. the time-series are conditioned on heat events (Fig. S12 a-c for wave-5 and Fig. S13a-c for wave-7). For this case we chose following notation: $ECA(h_{s,t}|A_w, h_{s,t}|A_w)$. Second, coincidence analysis is performed for all remaining weeks as well (i.e. conditioned on non-events, this we write as $ECA(h_{s,t}|\neg A_w, h_{s,t}|\neg A_w)$) shown in Fig. S12 d-f for wave-5 and Fig. S13 d-f for wave-7. When comparing coincidence rates between both, we find that heat events tend to co-occur more often when wave events are present, specifically for heat events that are wide-spread and of high temperature.

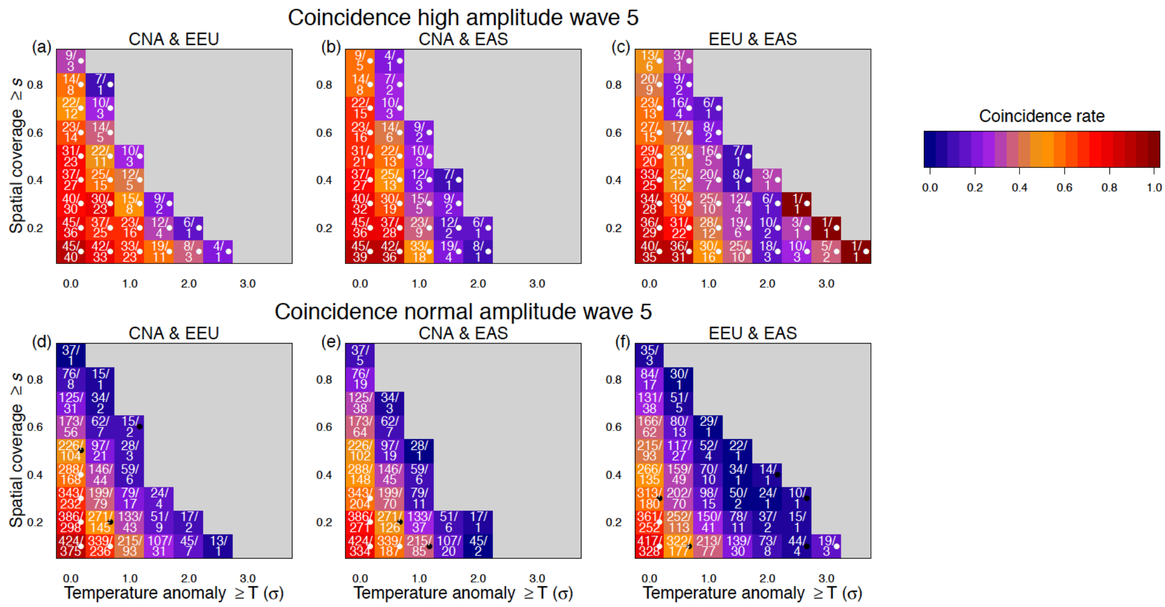

Figure S12. Coincidence rates of heat events in pairs of regions conditioned on wave-5 events. (a-c) Show the coincidence rates of heat events under the condition of high amplitude wave-5: $ECA(h_{s,t,i}|A_5, h_{s,t,j}|A_5)$ for regions associated with heat anomalies for wave-5. Statistical significance on a 0.99 (0.95) confidence level is indicated with a white (black) dot. Labels provide the number coinciding heat events in region r_i and r_j with A_5 and the number of heat events in region r_i coinciding with A_5. **(d-f)** Show the coincidence rates of heat events during all remaining weeks: $ECA(h_{s,t,i}|\neg A_5, h_{s,t,j}|\neg A_5)$. The probability of simultaneous extremes is significantly higher during weeks of amplified wave-5. Labels provide the number coinciding heat events in region r_i and r_j when wave-5 amplitude is below 1.5 σ and the number of heat events in region r_i with weeks of wave-5 amplitude below 1.5 σ.

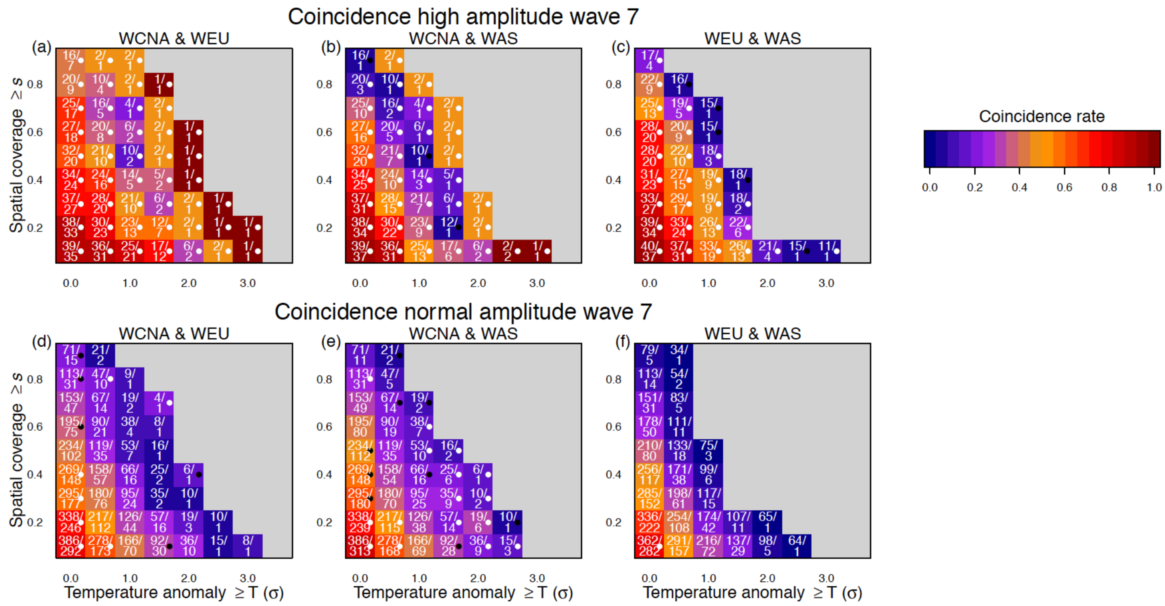

Figure S13. Coincidence rates of heat events in pairs of regions conditioned on wave-7 events. As in Fig. S12, but for wave-7.

Analysis of wave-6 and 8

Waves 6 and 8 do carry relevance for regional weather extremes, but as they do not exhibit a preferred phase (e.g. no particular phase locking, see Fig. 1), fewer statements can be made about the locations in which they occur (Figs. S1, S2, S16).

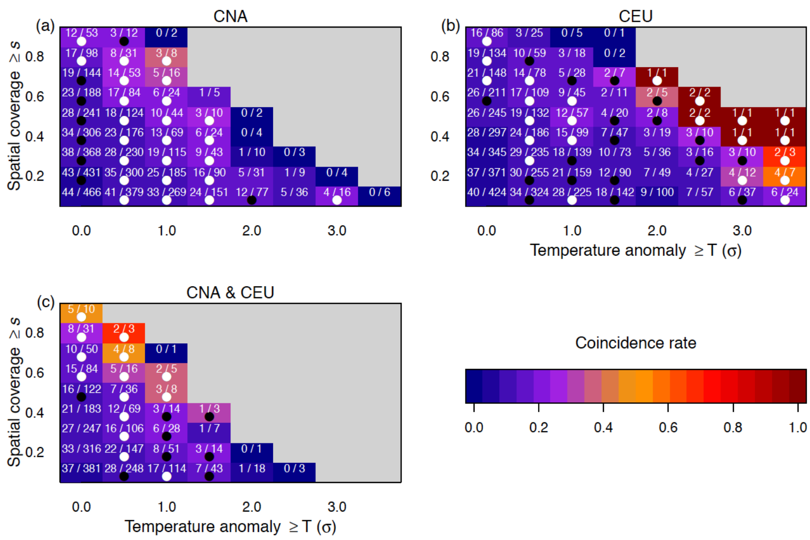

Figure S14. Coincidence of heatwaves in regions teleconnected by wave-6. As in Fig. S10, but for wave-6 and associated regions (see Fig. S16a for regions).

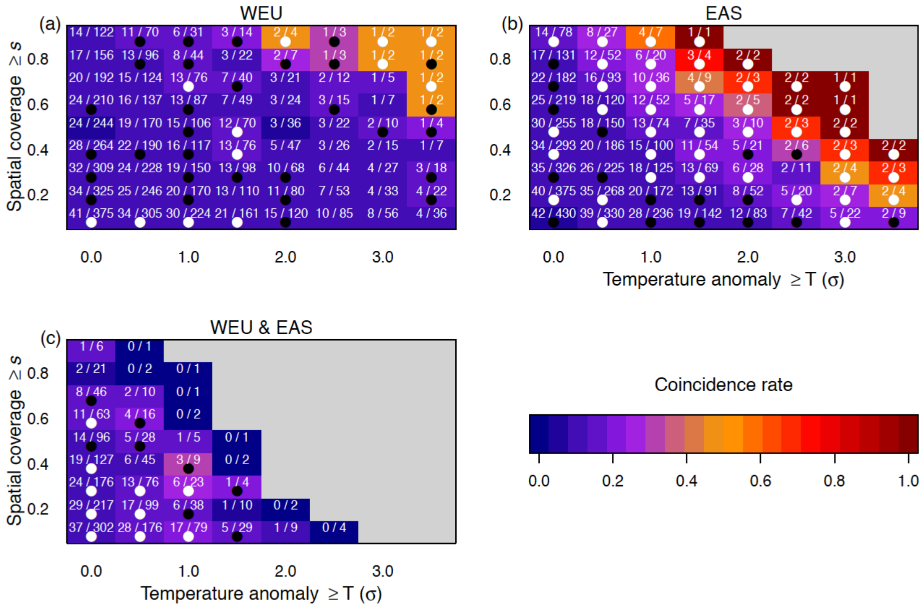

Figure S15. Coincidence of heatwaves in regions teleconnected by wave-8. As in Fig. S10, but for wave-8 and associated regions (see Fig. S16a for regions).

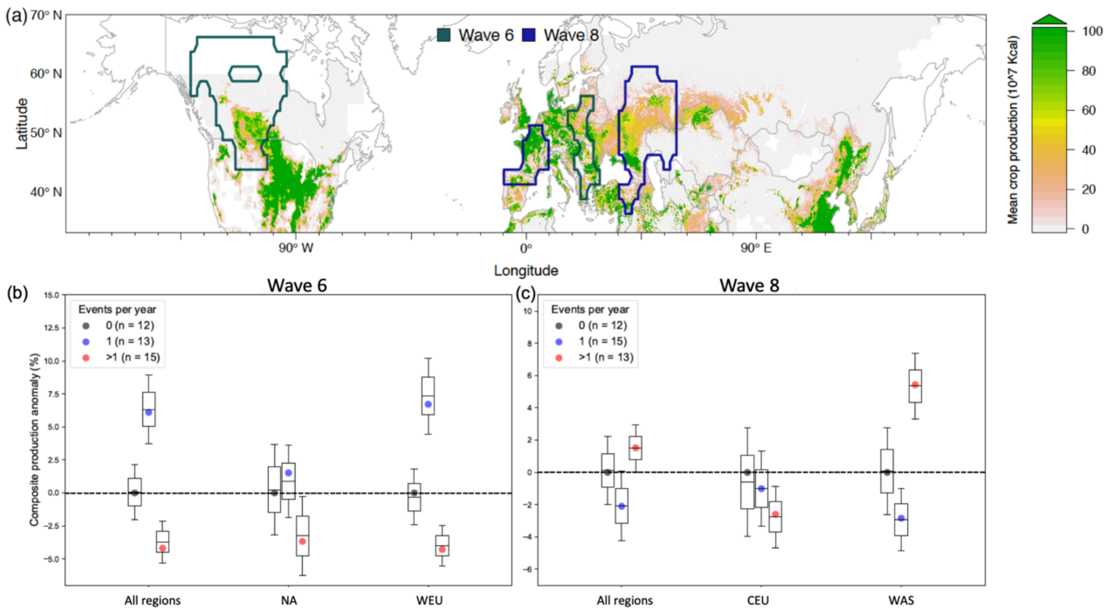

Figure S16. Crop production and teleconnected regions. As in Fig. 5, but for waves 6 and 8.

Supplementary tables

Table S1. Statistical significance of crop production anomalies associated with wave-5 and wave-7 events. P-values indicating statistical significance at the 95% confidence level are highlighted in red, p-values indicating statistical significance at the 90% confidence level are highlighted in light blue.

Wave- 5	Region:	All regions	CNA	EEU	EAS
p-value (1 event |>1 event)		0.37 | 0.18	0.04 | 0.18	0.5 | 0.23	0.5 | 0.34
Wave-7	Region:	All regions	WCNA	WEU	WAS
p-value (1 event |>1 event)		0.13 | 0.06	0.12 | 0.10	0.84 | 0.80	0.02 | 0.00

References

1. Kalnay et al., The NCEP/NCAR 40-year reanalysis project. *Bull. Am. Meteorol. Soc.*, 437–470 (1996).

2. D. K. Ray, N. Ramankutty, N. D. Mueller, P. C. West, J. A. Foley, Recent patterns of crop yield growth and stagnation. *Nat. Commun.* **3**, 1293–1297 (2012).

3. N. Siegmund, CoinCalc—A new R package for quantifying simultaneities of event series. *Comput. Geosci.* **98**, 64–72 (2017).

4. J. Donges, C. F. Schleussner, J. F. Siegmund, R. V. Donner, Event coincidence analysis for quantifying statistical interrelationships between event time series. *Eur. Phys. J. ST*. **225**, 471–487 (2016).

5. C. Lesk, P. Rowhani, N. Ramankutty, Influence of extreme weather disasters on global crop production. *Nature*. **529**, 84–87 (2016).